ACS OMEGA

http://pubs.acs.org/journal/acsodf

Article

Synergistic Release of Crop Nutrients and Stimulants from Hydroxyapatite Nanoparticles Functionalized with Humic Substances: Toward a Multifunctional Nanofertilizer

Ho Young Yoon, Jeong Gu Lee, Lorenzo Degli Esposti, Michele Iafisco, Pil Joo Kim, Seung Gu Shin, Jong-Rok Jeon,* and Alessio Adamiano*

Cite This: *ACS Omega* 2020, 5, 6598−6610

Read Online

ACCESS | Metrics & More | Article Recommendations | Supporting Information

ABSTRACT: The use of salt- or macro-sized NPK fertilizers is typically associated with low nutrient use efficiency and water eutrophication. Nanotechnology can overcome such drawbacks, but its practical application on a large scale is limited by (i) high costs and difficult scale-up of nanoparticle synthesis, (ii) questionable advantages over traditional methods, and (iii) health hazards related to nanomaterial introduction in the food stream and the environment. Here, we report on a novel biocompatible and multifunctional P nanofertilizer obtained by self-assembling natural or synthetic humic substances and hydroxyapatite nanoparticles using a simple and straightforward dipping process, exploiting the interaction between the polyphenolic groups of humic substances and the surface of nanohydroxyapatite. Pot tests using the as-prepared materials were performed on *Zea mays* as a model crop, and the results were compared to those obtained using commercial fused superphosphate and bare nanohydroxyapatites. A significant improvement, in terms of early plant growth, corn productivity, rhizosphere bacteria, and the resistance to NaCl-induced abiotic stresses, was achieved using hydroxyapatite nanoparticles assembled with humic substances. These effects were ascribed to the synergistic co-release of phosphate ions and humic substances, which are two types of plant-beneficial agents for crop nutrition and stimulation, respectively. The release patterns were proven to be tunable with the amount of humic substances adsorbed on the nanoparticles, inducing competition between humic-substance-driven phosphorous dissolution and block of water contact. Such positive effects on plant growth in association with its intrinsic biocompatibility, simple synthesis, and multifunctionality qualify this novel nanofertilizer as a promising material for large-scale use in the agronomic field.

INTRODUCTION

Since the last few decades, the agricultural lands utilized for intensive and irrigated farming have been suffering from several anthropogenic factors including the overuse of chemical NPK fertilizers, low crop nutrient use efficiency (NUE), leaching of soil organic matter, and soil salinization.[1−3] These factors adversely affected crop productivity and thus raised serious concerns due to competing demands for food to feed the ever-growing world population (projected to be 9.7 billion by 2050).[4] In this context, the development of nanotechnology-based fertilizers for crop nutrition has been suggested as an alternative tool to overcome the drawbacks arising from the current agricultural practices. Much effort has been thus devoted to design nanobased architectures for agronomical purposes. However, there is still a concern about the intentional utilization of nanoparticles for crop cultivation, as residual nanomaterials in crops and in the environment will eventually increase their exposure routes, causing possible bioaccumulation through the food chain and potential negative effects on human health. As an example, the work by Servin et al. has proved that nanosized TiO_2 particles in soils can accumulate into cucumber fruits, suggesting that the use of nanomaterials can potentially lead to bioamplification toward humans.[5]

Due to their biocompatibility and biodegradability, hydroxyapatite (HA, $(Ca_{10}(PO_4)_6(OH)_2)$) nanoparticles are ranked as one of the most popular candidates for agronomical

Received: December 18, 2019
Accepted: March 3, 2020
Published: March 16, 2020

https://dx.doi.org/10.1021/acsomega.9b04354
ACS Omega 2020, 5, 6598−6610

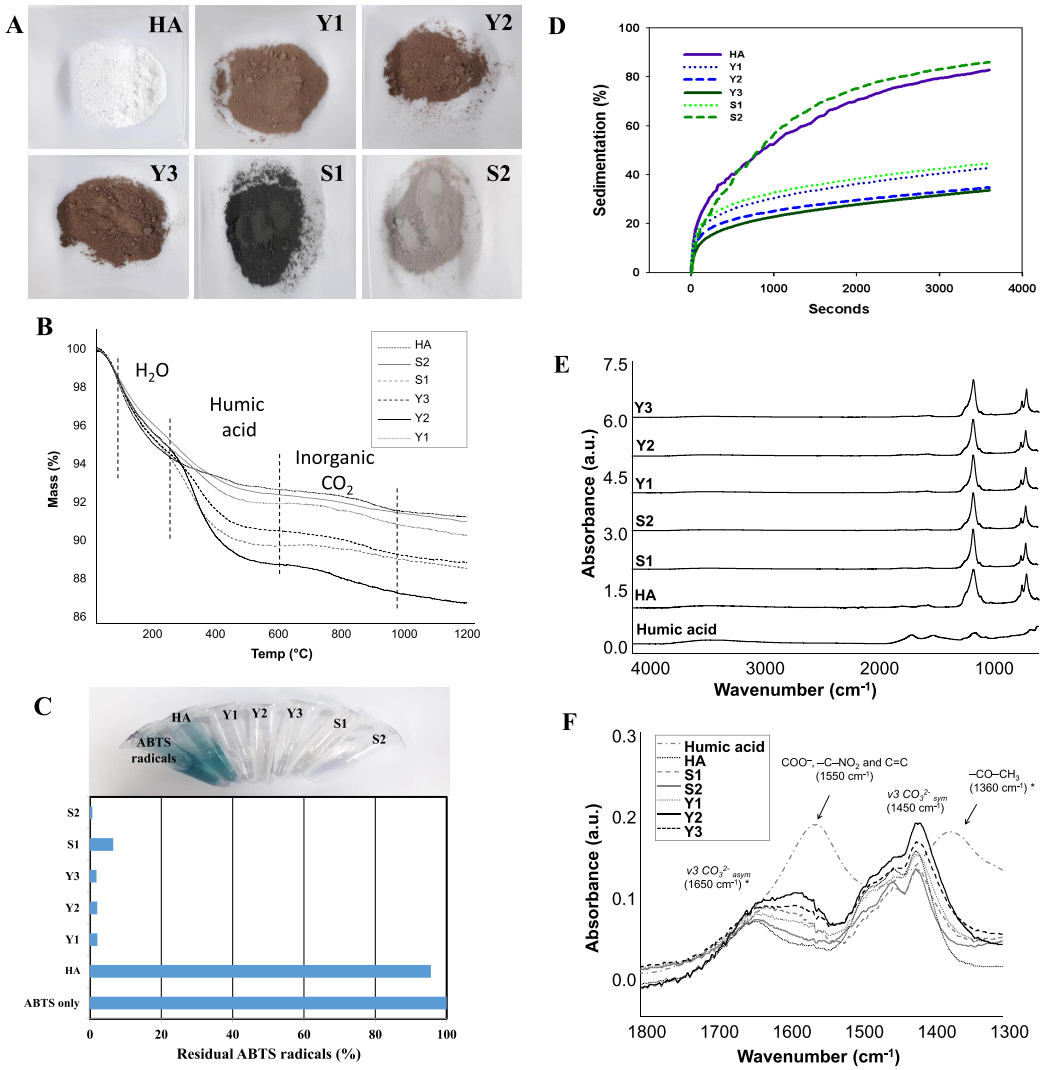

Figure 1. (A) Photographic images, (B) thermogravimetric analyses, (C) ABTS-based antioxidant capacities, (D) water sedimentation kinetics, (E) FT-IR spectra of pure and HS−HA nanoparticles, and (F) magnification of the FT-IR spectra in the region where the typical bands of HS (1800−1300 cm^{-1}) appeared. Abbreviation: HA, hydroxyapatite nanoparticles; Y1, Y2, and Y3, hydroxyapatite nanoparticles coated with commercial humic acids (0.01, 0.1, and 0.05 g/mL, respectively); S1 and S2, hydroxyapatite nanoparticles coated with phenolic polymers derived from catechol/gallic acid and catechol/ferulic acid, respectively.

applications. Moreover, HA dissolution into calcium and phosphate ions is very fast at low pH, indicating that stomach-acid-based digestion could completely prevent its accumulation in human organs.[6] HA nanoparticles can exploit their potential as fertilizers in two ways: (i) as controlled release fertilizers (CRFs) and (ii) as nanocarriers for the delivery of macro- or micronutrients. In the first case, the action mechanism is based on the water dissolution of HA nanoparticles, which are less soluble in aqueous media than commercial chemical fertilizers, thus allowing for a slower and more controlled release of P and other macro- or micronutrients in soils. In the second case, HA nanoparticles enter inside the plant tissues, where they can perform their action, retaining their structure or dissolving to release P and other nutrients.

Whether they are used as CRFs or as nanocarriers, the ability of HA nanoparticles to efficiently deliver nutrients to crops is hindered by their scarce mobility due to their low solubility in neutral and alkaline soils (i.e., pH > 7.0) and by their tendency to form large nanoparticle agglomerates, limiting their uptake by plant roots and leaves. A viable strategy to overcome these issues and improve HA nanoparticle bioavailability is to modify their surfaces with nontoxic and soil-friendly materials capable of increasing HA solubility and/or avoiding the formation of nanoparticle agglomerates. To this end, HA surface modification with several molecules such as citric acid and carboxymethyl cellulose (CMC) has been previously reported. More specifically, surface engineering of HA nanoparticles with citric acid has proven to be a facile way to modulate P releasing kinetics, allowing to provide optimal concentrations of P nutrients for crops during their growth.[6] In a paper by Liu and Lal, HA nanoparticles were coated with CMC to improve their colloidal stability in water and in turn to increase their mobility in soils.[7] Another approach reported in the literature is the decoration of HA nanoparticles with urea; however, even if the functionalization with amines improved the colloidal stability and increased the disaggregation of HA nanoparticles, in this case, the final aim was to decrease the solubility of urea and obtain a slower and more controlled release of nitrogen.[8]

https://dx.doi.org/10.1021/acsomega.9b04354
ACS Omega 2020, 5, 6598−6610

Table 1. Chemical Compositions of Pure and Humic-Coated Hydroxyapatite Nanoparticles Evaluated by ICP-OES and TGA[a]

	HA	S1	S2	Y1	Y2	Y3
Ca (wt %)	34.5 ± 1.7	32.9 ± 0.3	34.0 ± 0.1	31.8 ± 1.1	29.8 ± 1.3	32.5 ± 0.8
P (wt %)	16.0 ± 0.8	15.4 ± 0.1	16.2 ± 0.1	14.7 ± 0.5	13.5 ± 0.7	14.7 ± 0.3
CO_3 (wt %)	1.0 ± 0.1	1.0 ± 0.1	0.8 ± 0.1	1.0 ± 0.1	1.2 ± 0.1	1.2 ± 0.1
Ca/P (mol)	1.66 ± 0.01	1.65 ± 0.01	1.62 ± 0.01	1.68 ± 0.01	1.71 ± 0.02	1.71 ± 0.02
physisorbed water (wt %)	3.5 ± 0.2	2.1 ± 0.1	3.5 ± 0.2	3.0 ± 0.1	3.2 ± 0.2	3.5 ± 0.2
humic acid (wt %)		3.9 ± 0.2	1.2 ± 0.1	1.3 ± 0.1	4.9 ± 0.3	3.4 ± 0.2

[a]Data represent means ± SD (n = 3). Abbreviation: HA, hydroxyapatite nanoparticles; Y1, Y2, and Y3, hydroxyapatite nanoparticles coated with commercial humic acids (0.01, 0.1, and 0.05 g/mL, respectively); S1 and S2, hydroxyapatite nanoparticles coated with phenolic polymers derived from catechol/gallic acid and catechol/ferulic acid, respectively.

Table 2. DLS and BET Analyses of Pure and Humic-Coated Hydroxyapatite Nanoparticles[a]

	HA	S1	S2	Y1	Y2	Y3
ζ-potential (mV)	−1.7 ± 0.1	−18.5 ± 0.2	−8.4 ± 0.2	−19.8 ± 0.6	−31.7 ± 0.2	−22.8 ± 0.3
zeta average (nm)	3107 ± 40	414 ± 27	1947 ± 134	781 ± 84	688 ± 51	510 ± 43
SSA (m^2/g)	88.5 ± 4.0	85.1 ± 4.0	86.3 ± 4.2	94.3 ± 4.9	89.2 ± 4.2	93.4 ± 4.5

[a]Data represent means ± SD (n = 4).

Although sophisticated multifunctional materials applicable to nanomedicine have been continuously suggested,[9,10] to the best of our knowledge, very few trials have been reported to synthesize multifunctional nanomaterials capable of conducting multiple beneficial actions including crop nutrition and stimulation, soil amendments, and soil microbe flourishment. In this respect, humic substances (HSs), which are complex and recalcitrant organic polymers widespread in soils, are indeed a very interesting material by virtue of their ability to stimulate plants through activation of some gene sets, thus boosting their germination rates and abiotic stress resistance.[11−13] Moreover, oxygen-based functional groups easily identifiable in HS allow for versatile adsorption on solid surfaces[14] and may thus induce surface acidity, affecting the surface solubility of metallic oxides and HA.

Several proof-of-concept studies on HA-based nanofertilizers mainly reported on the size-related improvement in nutrient delivery and crop growth.[6,8,15−17] In this paper, we report on novel multifunctional, nontoxic, and soil-friendly nanocomposites consisting of HA nanoparticles functionalized with HS (HA−HS). HA−HS nanoparticles have a potential for tuning HA solubility through HS-driven surface acidity and co-releasing their crop nutritional and stimulatory components, i.e., phosphate ions and HS, respectively, in a synergistic and time-wise manner.

Self-assembly of water-dissolved natural and synthetic HS on the surfaces of HA nanoparticles was successfully performed by dipping the nanoparticles in aqueous HS solutions. Several analytical methodologies based on scanning electron microscopy (SEM), transmission electron microscopy (TEM), Brunauer−Emmett−Teller (BET) surface area, X-ray powder diffraction (XRD), dynamic light scattering (DLS), sedimentation kinetics, radical scavenging, size-exclusion chromatography, thermogravimetric analysis (TGA), and Fourier transform infrared spectroscopy (FT-IR) were used to characterize the synthesized materials. Finally, crop nutrition and stimulation induced by HA−HS were assessed using *Zea mays* as a model crop and were compared with the results obtained with unmodified nano-HA and commercial fused superphosphate (FS). The microbial community in *Z. mays*-cultivated soils was also analyzed to evaluate the effects of the investigated materials on the rhizosphere.

RESULTS AND DISCUSSION

The physicochemical properties of uncoated HA nanoparticles have been extensively described in previous works.[18−20] Since natural HSs have been successfully commercialized in agronomy and are easily obtainable in bulk from lignite and leonardite, commercial natural HSs were employed for the functionalization with HA.[11] HA nanoparticles were dipped in water solutions at different HS concentrations, where the reciprocal affinity of the two materials resulted in a fast and strong functionalization of the HA surface with the HS components to form HA−HS nanocomposites. As shown in the Y series of Figure 1A, the HA colors transformed from white to dark-brown after this step, owing to the well-recognized chromogenic features of HS.[21] More direct evidence of the adsorption was obtained by TGA analysis of different HA−HS nanoparticles (Figure 1B and Table 1). Significant mass decreases from 250 to 600 °C were clearly detected for all of the HA−HS nanoparticles and were ascribed to the thermal degradation of HS. As reported in the Y series of Table 1, the amount of HS determined by TGA was directly proportional to the HS concentration of the dipping solutions. It was previously demonstrated that versatile oxygen-based functional groups of HS allow for their binding onto surfaces of metallic oxides such as titania.[14] Similar binding mechanisms are likely to occur in the case of HA−HS due to the presences of Ca atoms on the surface of HA nanoparticles.

Radical scavenging activities and colloidal properties of HA−HS nanoparticles were assessed to verify whether HA nanoparticles are endowed with new features by functionalization with HS. The blue-colored 2,2′-Azino-bis(3-ethylbenzothiazoline-6-sulfonic acid) (ABTS) radical cations were significantly decolorized in the presence of HA−HS (Y series of Figure 1C), indicating that the radicals were efficiently reduced. It was previously shown that the electron-donating abilities of the phenolic groups of HS are involved in radical scavenging activity under aerobic conditions, suggesting that the observed decolorization is mainly due to the HS functionalization.[22] Sedimentation tests in aqueous media were performed to assess the ability of multiple hydrophilic groups of natural HS to stabilize aqueous suspension of HA nanoparticles, as previously reported with other mineral particles.[23] Figure 1D clearly shows that sedimentation kinetics

https://dx.doi.org/10.1021/acsomega.9b04354
ACS Omega 2020, 5, 6598−6610

of HA−HS nanoparticles of the Y series were much slower than that of uncoated HA. DLS data summarized in Table 2 also support this finding, as the zeta averages measured on Y samples were much lower than that of unmodified HA nanoparticles. Moreover, due to the large presence of oxygen-based functional groups in natural HS,[12−14] the ζ-potentials of these samples were much more negative than that of pure HA. Even if a linear correlation between the net charges and the zeta averages of nanoparticles in water dispersion was not observed, it is well known that the electrostatic repulsion between nanoparticles with the same electrical charge prevents their aggregation.[24] The improved colloidal properties of HA−HS in water with respect to bare HA would be particularly useful for agronomical applications, since several agrochemicals including pesticides are administered by crop watering.

Another evidence on the surface functionalization of the nanoparticles was revealed by the fact that all of the FT-IR spectra recorded on HA−HS (Y series of Figure 1E) presented the typical features of both HA and natural HS, as clearly visible from the magnified view in the 1300−1800 cm^{-1} range (Figure 1F). Within this region, the FT-IR spectra of HA were featured by bands ascribed to (ν3) CO_3^{2-} vibrations, while the spectra of natural HS were characterized by a band at 1550 cm^{-1}, attributed to COO^-, −C−NO_2, and C═C groups, and a band at 1360 cm^{-1} ascribed to the occurrence of −CO−CH_3 and possibly to nitrate groups.[25] The two bands of HS were superimposed to those of HA in the spectra of HA−HS, as highlighted by the occurrence of a broad shoulder at around 1600 cm^{-1} and a red shift of the (ν3) CO_3^{2-} symmetric band. Noteworthy, the intensity of these two signals was proportional to the amount of HS determined by TGA analysis of the Y series. Carbonate anions result from atmospheric CO_2 adsorbed on the surface and/or entrapped within the particles during the synthesis and storage. Their amount was evaluated according to the weight loss observed between 550 and 950 °C by TGA (Table 1) and was found to be similar for all of the samples.

The increased negative ζ-potential and the FT-IR analyses of HA−HS nanoparticles comply with the chelation of Ca^{2+} ions on the surface of HA nanoparticles by oxygen-based functional groups of HS. Data in the literature support this mechanism, as on the one hand HS are renown to have the ability to chelate metals,[26] while on the other it was previously proved that Ca^{2+} ions of apatite could be chelated by hydroxyl, carboxyl, and carbonyl groups of macromolecules such as chitin and chitosan.[27]

Oxidative polymerization of lignin-derived small phenolics gives rise to humiclike materials.[28] Bulk production of commercial HS relies heavily on natural coal resources, whose quantity and distribution are limited. To overcome this bottleneck, alternative uses of renewable lignin phenolics to obtain humic-like polymers having similar biological activity with respect to natural ones have been reported.[28] To this end, in this work, lignin-phenol-associated humic analogues were also employed to manufacture HA nanoparticles functionalized with HS synthesized from catechol and gallic acid or catechol and ferulic acid, named S1 and S2, respectively. Interestingly, synthetic HS exhibited similar results compared to the natural ones regarding coloration of HA nanoparticles, radical scavenging of ABTS, TGA, sedimentation kinetics, and FT-IR (S series of Figure 1 and Table 1), indicating that it is feasible to employ synthetic HS for nanoparticle functionalization. Like natural HS, oxygen-based hydrophilic groups derived from starting monomers (i.e., catechol, gallic acid, and ferulic acid) may play a role in the functionalization. Contrary to what was recorded for samples of the Y series, the amounts of HS revealed by TGA for S1 and S2 were unrelated to the concentrations of the dipping solutions (Table 1). In this respect, a major role is likely played by the structural variability of the HSs of S1 and S2, as it was previously shown that using different monomers in oxidative polymerization of lignin phenols leads to different physicochemical properties of the final polymer.[29]

SEM and TEM were employed to investigate the morphology and the size of HA nanoparticles. As shown in Figure 2, no significant differences between pure HA and natural and synthetic HS-coated particles were observed. All of the samples were composed of nanoparticles with needlelike morphologies, with length typically in the 75−125 nm size range and width in the 15−25 nm range. Since both SEM and TEM analyses were performed on nanoparticles in the dry

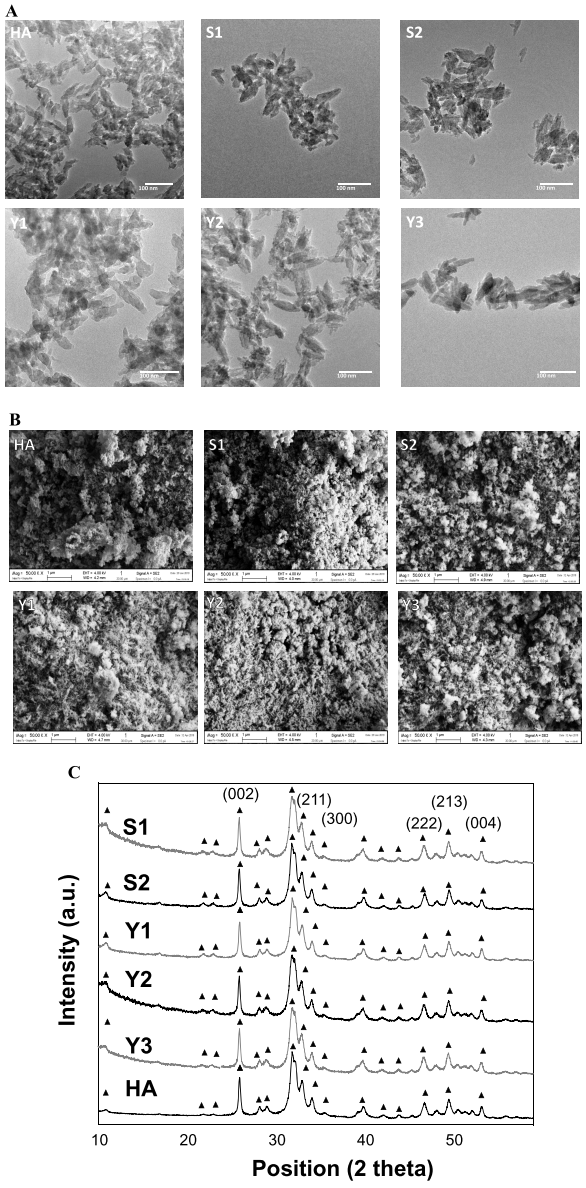

Figure 2. (A) TEM, (B) SEM, and (C) XRD of pure and humic-coated hydroxyapatite nanoparticles.

https://dx.doi.org/10.1021/acsomega.9b04354
ACS Omega 2020, 5, 6598−6610

state, the aggregation observed in these pictures was due to the prevalence of the electrostatic interactions of nanoparticles and it was not fully representative of the actual nanoparticle condition in aqueous dispersion. No external HS could be detected for any HA−HS, as commonly reported for nanoparticles coated with small amounts of organic polymers.[30]

SEM−EDX analyses were performed on HA and on the two samples containing the highest quantity of HS, namely, S1 and Y2. Generally speaking, the quantities of Ca and P were slightly higher than those detected by ICP-OES reported in Table 1 and were 35.5 ± 2.2, 35.0 ± 2.0, and 33.3 ± 4.5 wt % of Ca and 18.3 ± 1.3, 17.5 ± 1.3, and 17.7 ± 0.6 wt % of P for HA, S1, and Y2, respectively. However, despite the higher variability of EDX results with respect to ICP, the two sets of data were in good accordance. No statistically significant difference ($p < 0.05$, Student's t test) was recorded for Ca and P contents between HS-coated and bare HA nanoparticles. On the other hand, the amount of C was significantly higher in both samples S1 (5.5 ± 0.6 wt %) and Y2 (8.3 ± 4.2 wt %) with respect to HA (2.8 ± 0.5 wt %). As C is the main element of HS, this increase is ascribed to its presence on the surface of nanoparticles, while the amount of C detected for bare HA nanoparticles was mainly due to the presence of organic impurities. Finally, no differences could be found between the C contents of S1 and Y2, indicating that these nanoparticles feature similar amounts of HS on their surface.

Consistently with the SEM and TEM analyses, the XRD patterns collected on HA−HS (Figure 2C) were also very similar to those collected on uncoated HA and featured broad and poorly defined peaks typical of nanocrystalline apatite that can be indexed according to the crystallographic features of hydroxyapatite (JCPDS no. 09-432). These results support that the coating methods employed did not have any effect on the crystal structure of HA nanoparticles (Figure 2C).

Previous agronomical studies have clearly demonstrated that supplying HS to crops results in the increases in mobile P in soils, thus enhancing crop productivity.[31,32] This inspired us to check whether it is possible to tune P solubilization kinetics from HA nanoparticles by modifying their surface with natural and synthetic HS. Compared with uncoated HA nanoparticles, HA−HS exhibited a significant enhancement in the release of phosphate ions (Figure 4), but this increase was not proportional to the amount of HS (Figure 3 and Table 1). This is probably due to two concomitant phenomena: (i) an increase in the surface acidity of HA nanoparticles determined by the presence of oxygen-based functional groups of HS adsorbed onto them and (ii) a reduction of the contact surface between water and HA nanoparticles. The first determines a faster dissolution of HA nanoparticles, i.e., a faster release of phosphate ions, while the second hampers the interaction between the HA surface and water molecules, slowing down P solubilization. Hence, to find the right balance between surface acidity and water passage in the HS−HA interface might be a critical factor in optimizing P releasing rate.

Desorption of humic structures from solid surfaces has been described in previous works suggesting that physisorption is the main mechanism governing humic-based solid attachments.[33] The desorption kinetics of HS from the nanoparticles were thus monitored through UV−vis spectrometry. Generally speaking, there is a fair agreement between HS release kinetics (Figure 5) and HS amounts determined by TGA for all of the samples (Table 1). Size-exclusion chromatography was then

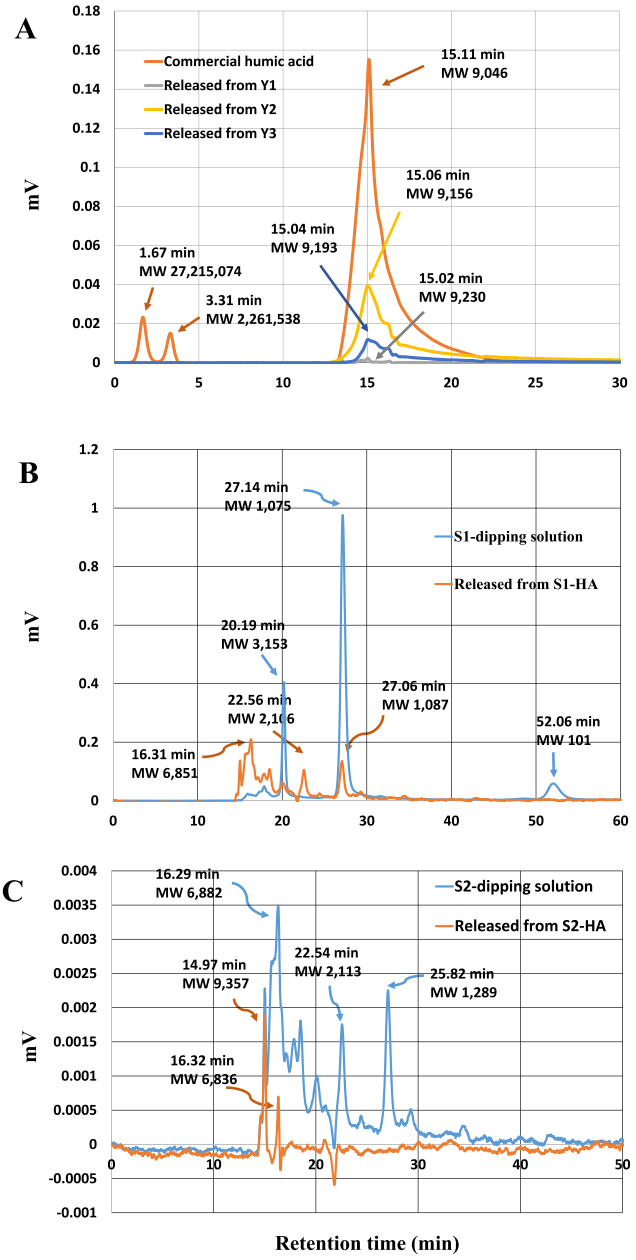

Figure 3. Size-exclusion chromatography of humic substances derived from either dipping solutions or desorption from hydroxyapatite nanoparticles. Analysis of (A) commercial humic acids and synthetic phenolic polymers derived from (B) catechol/gallic acid and (C) catechol/ferulic acid.

employed to characterize humic components released from HA−HS surfaces as well as those in the original dipping solution. As shown in Figure 3, HSs with molecular weights around 10 000 were detached from samples of the Y series, while the molecular weights of the HS detached from samples of the S series were more diversified. Muscolo et al. suggested that HSs with molecular weights of several thousands of Da are involved in direct plant stimulations due to their adsorption onto plant root surfaces, supporting that the released humic components from HA nanoparticles can act as a direct plant stimulant.[34] The released HSs are also able to chelate calcium ions derived from the dissolution of HA nanoparticles, thus hampering the re-precipitation of calcium phosphate.[35] This inhibitory action combined with the surface acidity of HS

https://dx.doi.org/10.1021/acsomega.9b04354
ACS Omega 2020, 5, 6598−6610

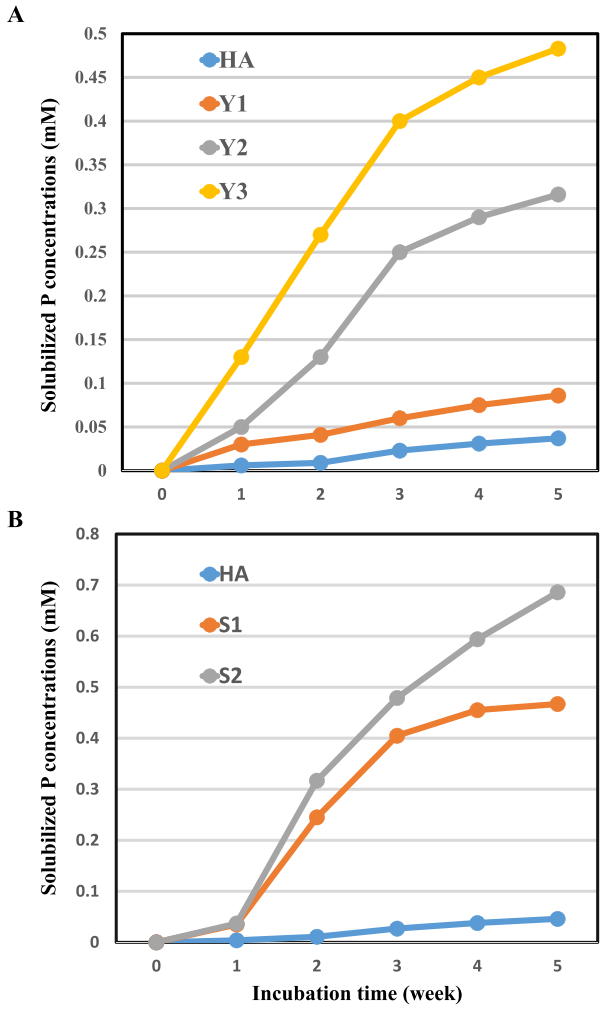

Figure 4. Solubilized P kinetics released from pure and humic-coated hydroxyapatite nanoparticles. (A) Natural and (B) synthetic humic substances. P contents measured on a weekly basis were cumulated.

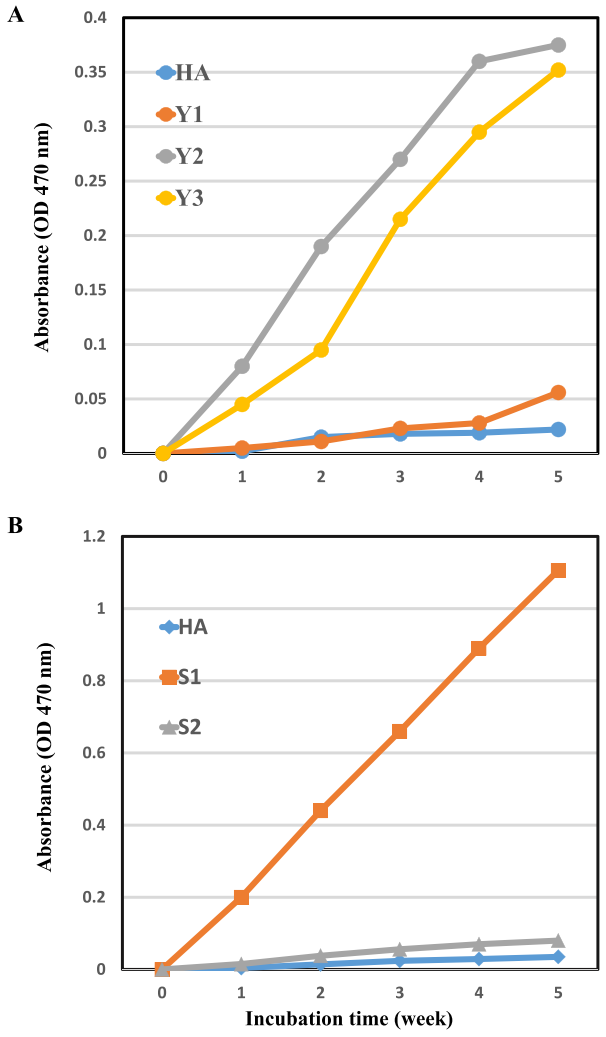

Figure 5. Desorption kinetics of humic substances from pure and humic-coated hydroxyapatite nanoparticles. (A) Natural and (B) synthetic humic substances. Humic contents measured on a weekly basis were cumulated.

could be a key to tune phosphorus releasing kinetics from HA−HS nanoparticles. In addition, these results strongly indicate that HA−HS nanoparticles can be used for the co-delivery of crop nutrients (i.e., phosphate ions) and stimulants (i.e., HS) toward rhizospheres in a time-wise and synergistic manner. Finally, this co-release could maximize the agronomical applicability of our nanofertilizers compared with previously developed ones exclusively focusing on nutrient supply.[6,8,15−17]

Since maize (i.e., *Z. mays*) is one of the most common food crops in the world,[36] it was selected as a model to test the agronomical effectiveness of our HA−HS nanoparticles. Co-releasing features of phosphate ions and HS were expected to promote both growth and stress resistance, as P is a plant macronutrient and HSs are known to stimulate several gene sets of plants related to stress relieving.[34,37] Hence, the extents of early growth, corn productivity, and resistance to NaCl induced by HA−HS nanoparticles were evaluated and compared with those achieved using pure HA and commercial FS featuring double-releasing mechanisms due to the presence of fast dissolving P salts and slow-releasing P solids.

In the early growth experiments, a similar crop height determined by the maize leaf length was recorded in all of the conditions, while the growth of the crop stems was remarkably higher in plants treated with HA−HS nanoparticles, thus resulting in a significant increase of their fresh and dry weights compared with those measured in plants treated with pure HA nanoparticles and commercial FS (Figure S1). Early growth rates of maize per P unit were then assessed on the basis of the chemical composition of the tested materials determined by ICP-OES reported in Table 1 (Figure 6A,B; the content of P element in commercial FS was based on the product instruction). Y3 and S2 showed superior fertilizing activities than commercial FS as well as unmodified HA in terms of units of P supplied. It was previously reported that HSs present in soils facilitate plant uptake of metallic micronutrients such as iron.[38,39] To evaluate whether metallic elements and P were uptaken more by maize plants treated with HA−HS nanoparticles than by plants treated with FS and HA nanoparticles, the detailed contents of K, Ca, Fe, and P in the biomass were assessed by ICP-OES analyses. As shown in Figure 6C, no significant differences were identified among the treatment groups. This result is probably related to the amount of HS in HA−HS nanoparticles, which is much smaller than the typical amount of HS used in conventional humic treatments for agronomical purposes.[39] Moreover, the interaction with HA

https://dx.doi.org/10.1021/acsomega.9b04354
ACS Omega 2020, 5, 6598−6610

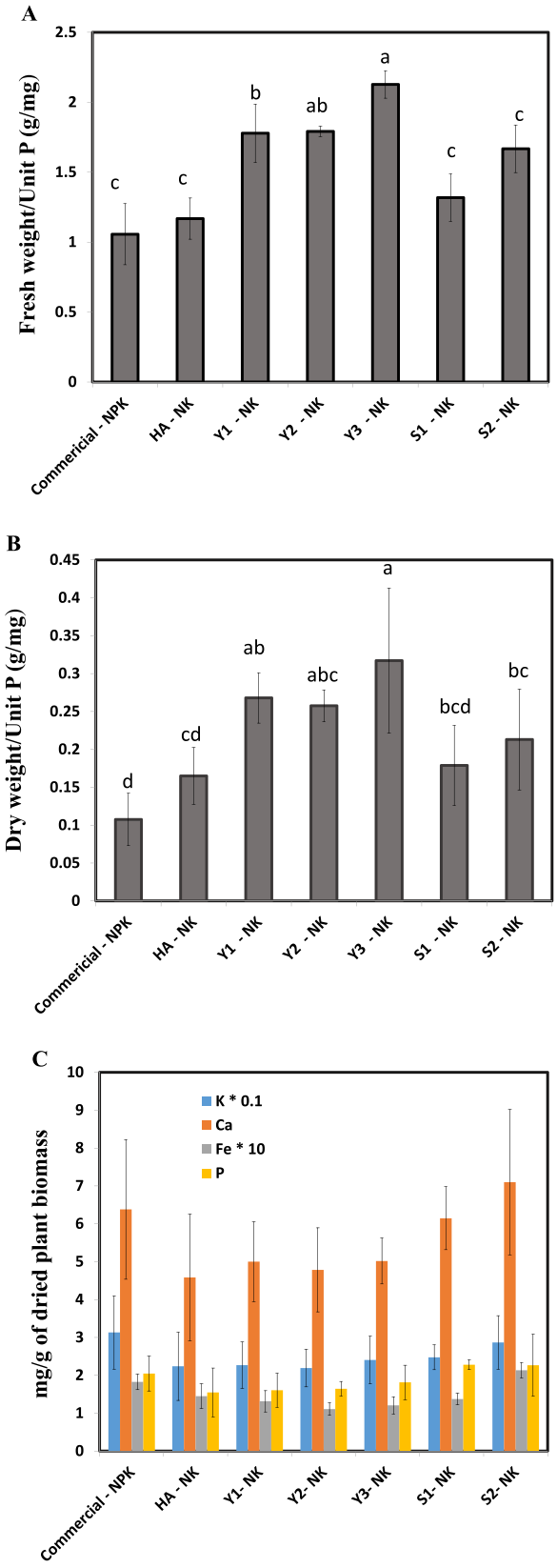

Figure 6. (A) Fresh and (B) dry weights of *Z. mays* at an early growth stage per unit of P supplied. The same kind and amount of NK fertilizers were supplied in all of the conditions. (C) Contents of K, Ca, Fe, and P per gram of dried *Z. mays* harvested at an early growth stage. Data represent means ± SD (n = 3), and statistical analysis was based on LSD (p < 0.05).

and the consequent time-wise release of HS reasonably lead to a further decrease in the concentration of free HS in the soil environments.

Rhizosphere microbiome is known to positively affect crop productivity by aiding plant nutrient uptake and inducing the plant defense mechanism.[40] HSs are able to immobilize plant nutrients and to act as electron donors/acceptors for microbial respiration.[32,41] In fact, supplying HS in the soil can lead to increases in microbial biomass, suggesting that these materials are involved in microbial proliferation.[42] Moreover, HS can exert positive effects on the rhizosphere formation by virtue of their ability to boost root genesis and elongation.[13] Since carbon-rich root exudates are able to attract plant-beneficial microbes and root surfaces provide physical spaces for mutualistic microbes including mycorrhizae and rhizobia, HS-driven root growth stimulation could be linked to enhanced rhizosphere formation, which in turn affects soil microbiome. To check this possibility, microbial community structures in soil rhizospheres treated with commercial FS, uncoated HA nanoparticles, and the most promising materials selected among the HA–HS samples (i.e., Y3 and S2) were evaluated through metagenomic analyses of bacterial 16S ribosomal DNA sequences. As shown in Figure 7, *Rivulariaceae*

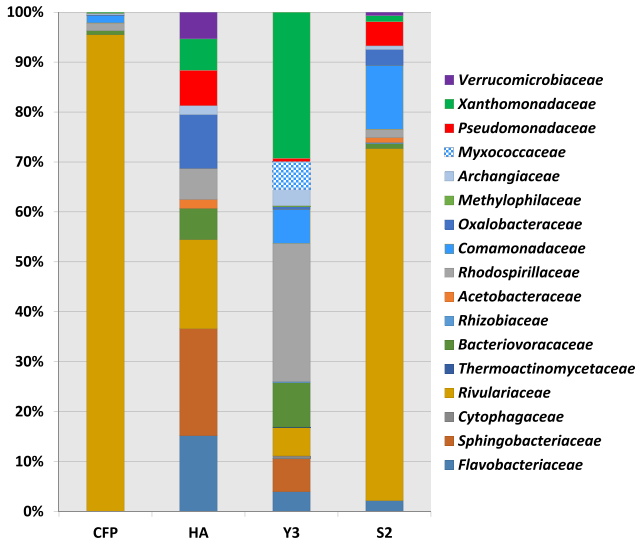

Figure 7. Soil microbiome analyses of *Z. mays* rhizospheres in soils treated with commercial fused superphosphate and pure and humic-coated hydroxyapatite nanoparticles. The same kind and amount of NK fertilizers were supplied in all of the conditions. Abbreviation: CFP, commercial fused superphosphate.

belonging to cyanobacteria identifiable in croplands[43] was dominant (>95%) in FS-treated soils, whereas other treatment groups showed much more diverse microbial compositions.

Different bacterial OTUs between pure and humic-coated HA nanoparticles were also detected. *Xanthomonadaceae* and *Rhizobiaceae*, which are known to be involved in symbiotic plant–microbe interactions,[44,45] were more abundant in Y3 than in S2 (Table S2). As shown in Table S3, the highest number of bacterial OTUs was detected for the Y3 treatment and matched the bacterial species typically associated with plant rhizosphere. The detected OTU patterns in association with the enhanced root genesis observed for HS–HA treatments (Figures S1 and S2) highlight the occurrence of a

https://dx.doi.org/10.1021/acsomega.9b04354
ACS Omega 2020, 5, 6598–6610

Table 3. Maize Productivity and Phosphorus Use Efficiency on Treatment with Commercial Fused Superphosphates and Pure or Humic-Coated Hydroxyapatite Nanoparticles[a]

	maize productivity (Mg/ha)					phosphorus uptake (kg/ha)					
treatment	grain	leaf	stem	root	sum	grain	leaf	stem	root	sum	ARE (%)
NK	12.0d	13.3c	11.4d	7.7c	44.4	3.0c	0.9b	1.1d	0.4b	5.4d	
commercial P—NK	13.8bc	14.7bc	15.9bc	8.6b	53.0	3.6b	1.3b	3.7a	0.1b	8.7b	27.5c
HA—NK	13.1c	14.1c	13.5cd	7.2c	47.9	3.5b	1.1b	2.0c	0.7a	7.3c	13.3d
S2—NK	14.3b	15.9ab	16.4b	9.2b	55.8	4.7a	2.5a	2.2bc	0.9a	10.4a	36.2b
Y3—NK	16.2a	16.5a	20.5a	11.4a	64.6	4.5a	3.0a	2.8b	1.0a	11.3a	48.0a

[a]Data represent means ± SD (n = 3), and statistical analysis was based on LSD ($p < 0.05$). The same amount of NK fertilizers was used in all of the conditions. Phosphorus uptake and ARE were evaluated by phosphorus contents of soils, harvested crops, and fertilizers. Abbreviations: Commercial P, fused superphosphate; ARE, apparent recovery efficiency by difference (i.e., the amount of nutrient uptake (treatment − control)/the amount of nutrient treated).

positive effect of HS slow release on the flourishing of rhizosphere bacteria.

To further investigate the growth promotion of maize by Y3 and S2, maize growth experiments were prolonged until the crop was fully grown. As shown in Table 3, grain weights derived from Y3 and S2 treatments were higher than from treatments with bare HA nanoparticles and commercial FS. Remarkably, the phosphorus use efficiency of Y3 and S2 was proven to be much higher during the whole maize growth cycle, indicating that the low plant NUE achieved with the use of conventional fertilizers could be overcome with the use of humic-coated nanosized ones. The much lower phosphorus uptake of pure HA nanoparticles evidences the important role played by the functionalization with HS to overcome the limits of HA-based nanofertilizers, especially their scarce solubility at pH > 7 and the tendency of HA nanoparticles to form large aggregates in the dry state. In addition, it can be concluded that the P uptake efficiency of maize increased with increasing cultivation periods in plants treated with HS−HA nanoparticles (Figure 6C and Table 3). Moreover, as soil P availability affects leaf developments and the leaf area index,[46] this increase could be related to the higher P availability in the soil obtained with HS-coated nanoparticles, which would eventually induce faster carbon fixation, resulting in increased biomass weights (Figure 6A,B).

The salt resistance of *Z. mays* under the various treatments was compared to evaluate whether HS−HA nanoparticles display multifunctional properties. As shown in Figure S2A, under salt-induced stress conditions, the growth of crops treated with commercial FS was very slow and plant leaves readily turned gray, suggesting that their chlorophyll was completely destroyed. On the contrary, maize plants treated with pure HA and HS−HA retained their normal appearances, determining in turn a significant growth enhancement in terms of crop height and fresh and dry weights with respect to the group of plants treated with FS (Figure S2B,C). Crop growth per unit of administered P under salt-induced stress finally highlighted that humic-coated nanoparticles had much higher stimulating activities than commercial FS and bare HA nanoparticles (Figure 8).

In this regard, it is important to note that abiotic stress relieving for crop growth was found to be related to P availability in soil.[47] However, the fact that FS is very capable of providing P nutrients to crops supports that the nutrient supply is not enough to fully compensate for the salt-related abiotic stresses. On the other hand, when treated with HS, plant roots are able to modulate the expression level of high-affinity K^+ transporter 1 and thus mitigate salt-induced toxicity.[37] The combined action of co-released HS and phosphorus ions reported in our study was thus able to efficiently mitigate salt-induced adverse effects on maize growth. Further studies focusing on synergistic stimulatory mechanisms driven by the co-presences of humic materials and P-related nutrients for crop salt resistance should be addressed

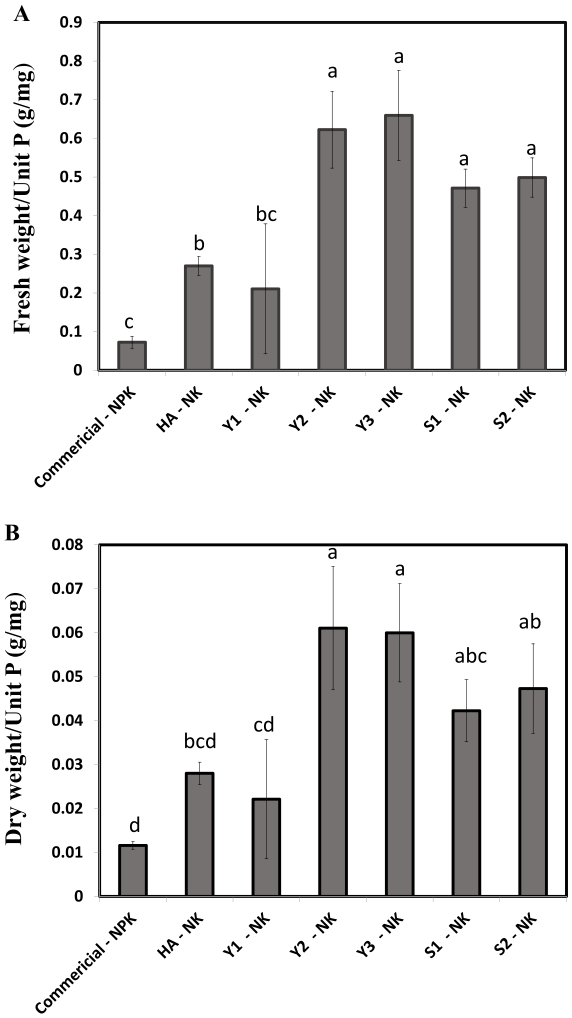

Figure 8. (A) Fresh and (B) dry weights of *Z. mays* at an early growth stage per unit of P supplied in the presence of NaCl. The same kind and amount of the NK fertilizer were supplied in all of the conditions. Data represent means ± SD (n = 3), and statistical analysis was based on LSD ($p < 0.05$).

https://dx.doi.org/10.1021/acsomega.9b04354
ACS Omega 2020, 5, 6598−6610

Scheme 1. Proposed Sorption Mechanisms between Humic Substances and Hydroxyapatite Nanoparticles[a]

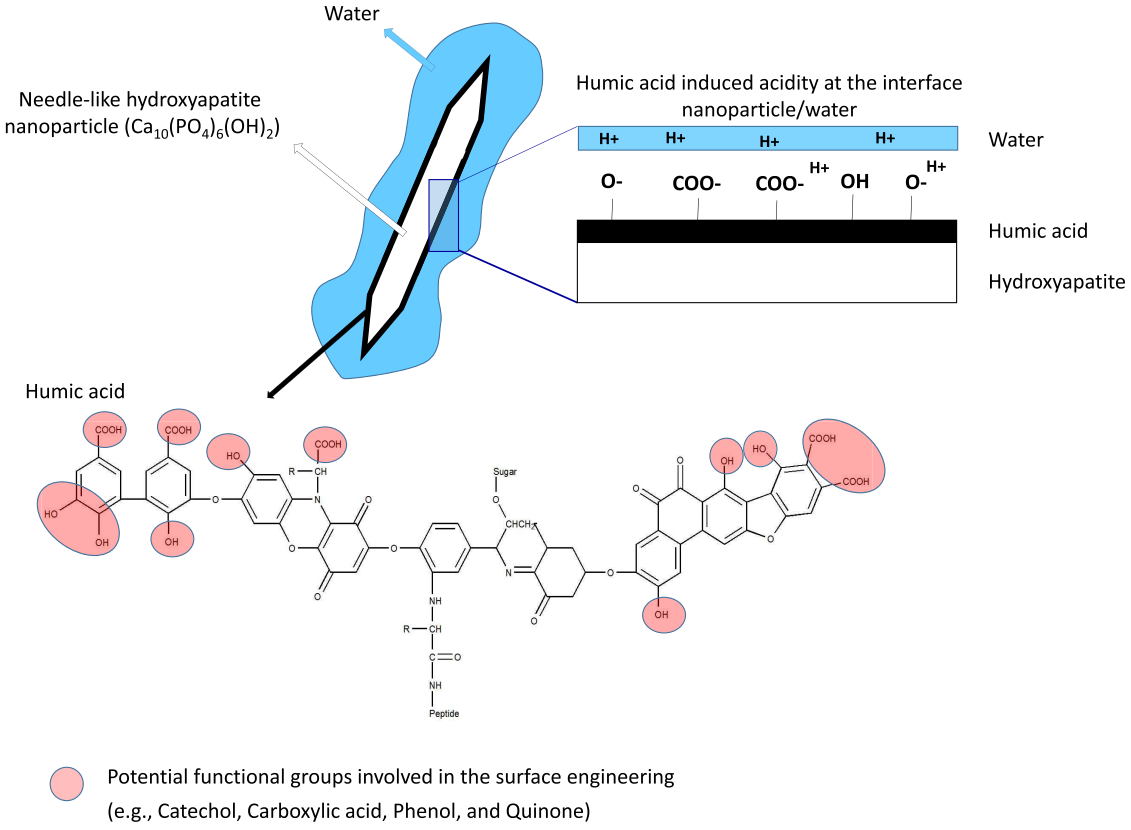

[a]The assumed structure of humic acids is from Vekariya et al.[14] The organic functional groups of humic acids potentially involved in the attachment to the hydroxyapatite surfaces are highlighted.

to fully figure out the multifunctionality of these HS−HA nanocomplexes.

CONCLUSIONS

We proved that multifunctional biocompatible and biodegradable nanoparticles for agronomical purposes could be readily synthesized by dipping of nano-HA in a water solution of HS. Remarkably, fertilizing- and abiotic-stress-relieving capacities in *Z. mays* crops treated with our multifunctional nanofertilizers were significantly enhanced compared with commercial FS as well as with unmodified HA nanoparticles. These effects were proven to be derived from the adsorption of HS on the surface of nanoparticles, where they played a double role during P solubilization. In fact, on the one hand, the increase in the surface acidity determined by humic substances stimulated the dissolution of hydroxyapatite nanoparticles, and on the other hand, the presence of HS on the surface of the nanoparticles acted as a physical barrier for water contact. The binding between HA nanoparticles and HS enabled their reversible detachment, allowing a time-wise and synergistic co-release of crop nutrients and stimulants, which in turn improved crop nutrition, abiotic stress relief (Scheme 1), and rhizosphere bacteria growth. Overall, these findings strongly support that multifunctional nanomaterials can be obtained by simple and easily scalable processes, and their large-scale use in agriculture could start in the near future.

EXPERIMENTAL SECTION

Materials. Calcium hydroxide ($Ca(OH)_2$, 95%), catechol (99%), *Trametes versicolor* fungal laccases (1.03 U/mg), vanado-molybdate (p.a., for phosphate determination), nitric acid (HNO_3, puriss p.a. ≥65%), hydrochloric acid (HCl, puriss p.a. ≥37%), and potassium bromide (KBr, FT-IR grade, ≥99% trace metal basis) were purchased from Sigma-Aldrich. Ferulic acid (98%) and ABTS (98%) were purchased from Fluka. Sodium azide (NaN_3, 99%), sodium dihydrogen phosphate (NaH_2PO_4, 99%), and sulfuric acid (H_2SO_4, 95%) were obtained from Daejung Chem (Korea). Phosphoric acid (H_3PO_4, 85%), natural HS (humic acid, >70 wt % humic matter), gallic acid hydrate (98%), and poly(styrene sulfonate) standard materials were purchased from Merck, Mycsa AG (Texas), Tokyo Chemical Industry (TCI, Japan) and PSS-Polymer (Maryland), respectively. Urea, potassium chloride (KCl), and FS were purchased from Namhae Chemical Corporation (Korea), Enpico Corporation (Korea), and Nonghyup Corporation (Korea), respectively. Perchloric acid ($HClO_4$), an Agencourt AMPure XP reagent bead, and a FastDNA Spin Kit were obtained from Samchun Chem (Korea), Beckman Coulter (Italy), and MP Biomedicals (California), respectively. Unless otherwise specified, ultrapure water (0.22 μS, 25 °C, Milli-Q, Millipore) was used in all of the experiments. All of the reagents were used as received without any further purification.

Synthesis of Hydroxyapatite Nanoparticles. HA nanoparticles were synthesized by a neutralization method already reported by Adamiano et al.[18] with some modifications. Briefly,

https://dx.doi.org/10.1021/acsomega.9b04354
ACS Omega 2020, 5, 6598−6610

10 g of $Ca(OH)_2$ was added to 100 mL of water and then stabilized at room temperature under constant stirring at 400 rpm for 30 min (initial pH ∼ 12.0). A solution obtained by mixing 8.87 g of H_3PO_4 with 30 mL of water was added dropwise into the $Ca(OH)_2$ suspension at room temperature. The molar ratio between calcium and phosphorous was set to 1.67 and kept constant for all of the syntheses. Once the simultaneous dropwise addition of phosphoric was completed, the solution was kept at room temperature under constant stirring at 400 rpm for 3 h and then left still overnight (final pH ∼ 7.0). Finally, the powder was repeatedly washed with water and then air-dried at 40 °C until constant weight.

Functionalization of Hydroxyapatite Nanoparticles with Natural and Synthetic Humic Substances. Natural HS was dissolved in autoclaved distilled water at three different concentrations (i.e., 0.01, 0.1, and 0.05 g/mL). After removing water-insoluble HS through centrifugation (13 000 rpm, 10 min), HA nanoparticles (1 g) were added to the humic solution (9.9 mL), vigorously vortexed, and further incubated under agitation on a roller (60 rpm, 20 min) at room temperature. HS-coated HA nanoparticles were isolated via centrifugation (13 000 rpm, 10 min), and the pellets were vortexed with autoclaved distilled water to remove loosely attached HS. HA was recovered by centrifugation, and the resulting pellet was dried at 55 °C and ground in a mortar. Samples obtained by soaking HA nanoparticles in the solutions at 0.01, 0.1, and 0.05 g/mL of natural HS were named Y1, Y2, and Y3, respectively. Synthetic HSs were obtained via enzymatic polymerization of lignin-derived phenolics as described previously.[28] Briefly, either catechol (0.1 g) and gallic acid (0.1 g) or catechol (0.1 g) and ferulic acid (0.1 g) were polymerized by single-electron oxidation using fungal *T. versicolor* laccases (2.65 mg) in 100 mM sodium acetate buffer containing 20% EtOH (40 mL) at room temperature overnight. HA nanoparticles were then immersed in the resulting solutions, following the same procedure already described for the natural HS coating. The HA samples coated with the polymers from catechol/gallic acid and catechol/ferulic acid were finally named S1 and S2, respectively.

Radical Scavenging and Water Sedimentation Kinetics. The extent of radical scavenging driven by bare HA or HA−HS nanoparticles was based on ABTS radical decolorization. The blue ABTS radical cations were produced through fungal-laccase-catalyzed single-electron oxidation of ABTS, followed by ultrafiltration (5000 MWCO, Vivaspin 15R, Sartorius). The absorbance of the ultrafiltrated radical solution at 420 nm was adjusted to 1.6 by adding distilled water. The radical solutions (1 mL) were then incubated overnight with bare HA or HA−HS nanoparticles (1 mg) under agitation on a roller (60 rpm). After centrifugation (13 000 rpm, 10 min), the absorbance of the supernatants was measured at 420 nm and subtracted with the absorbance of the control, consisting in a water dispersion of pure and humic-coated HA nanoparticles without ABTS.

Size-Exclusion Chromatography. Size-exclusion analysis of HS was performed using a PolySep GFC-P3000 300 × 7.80 mm^2 (Phenomenex), preceded by a PolySep GFC-P 35 × 7.80 safety guard (Phenomenex) with high-performance liquid chromatography (a Waters 2695 system with a Waters 996 photodiode array detector) as described previously.[12] Syringe-filtered (0.45 μm PTFE, Advantec) humic solutions used for the dipping of HA nanoparticles were analyzed with a mobile phase of 0.1 M NaH_2PO_4 solution buffered at pH 6.5 containing 4.6 mM NaN_3. Their separations were then monitored at 280 nm with a 0.6 mL/min flow rate. Poly(styrene sulfonate) showing 6520, 14 900, and 145 000 M_w (Da) and ferulic acid were employed to make a calibration curve as performed previously.[12] The same procedure was followed to analyze the HS detached from coated HA nanoparticles in distilled water (30 mg/mL) after 1 day of incubation at room temperature.

Co-release of Phosphate Ions and Humic Substances. Pure and humic-coated HA nanoparticles (1 g) were suspended in distilled water (40 mL) and placed under agitation on a roller (60 rpm). A 1 mL aliquot of the solutions was taken for the quantification of phosphate ions and humic contents each week. Subsequently, fresh autoclaved distilled water was re-supplied weekly to prevent the saturation of the soluble materials in the given water volume as well as to fully mimic rhizosphere environments, where solubilized nutrients are uptaken by plants and microbes. HS desorption kinetics from HS−HA nanoparticles in water was quantified by the spectrometric detection at 470 nm of the supernatant recovered by centrifugation (13 000 rpm, 10 min) of the 1 mL aliquot. Phosphate release was determined by a vanado-molybdate colorimetric method at 470 nm performed on the same aliquot by subtracting the absorbance values ascribed to HS desorption. The release patterns of phosphate ions and humic structures were recorded in duplicate, and no significant difference in the patterns was observed.

Chemical Analysis. Calcium and phosphate contents of pure and humic-coated HA nanoparticles were determined using inductively coupled plasma-optical emission spectrometry (ICP-OES) on a Liberty 200 spectrometer (Agilent Technologies 5100 ICP-OES, Santa Clara, CA) employing wavelengths of 422.673 (Ca) and 213.618 nm (P). A total of 20 mg of dried samples was dissolved in 50 mL of 2 wt % HNO_3 or 2 wt % HCl solutions prior to the analysis.

X-ray Diffraction Analysis. The phase composition of each powder was determined by XRD with a D8 Advance diffractometer (Bruker, Karlsruhe, Germany) equipped with a Lynx-eye position-sensitive detector using Cu Kα radiation (λ = 1.54178 Å) generated at 40 kV and 40 mA. XRD spectra were recorded in the 2θ range of 10−60° with a step size (2θ) of 0.04° and a counting time of 0.5 s.

Fourier Transform Infrared Spectroscopy Analysis. FT-IR spectra of dried samples in KBr disks were recorded at room temperature using an FT-IR Nicolet 380 from Thermo Electron Corporation working in the range of wavenumbers 4000−400 cm^{-1} at a resolution of 2 cm^{-1}. A finely ground, approximately 0.05% (w/w) mixture of the sample in KBr was pressed into a transparent disk using a hydraulic press and applying a pressure of about 670 MPa.

ζ-Potential and Size Measurements. ζ-Potential distributions of dried powders suspended in water were measured by dynamic light scattering (DLS) with a Zetasizer Nano ZS (Malvern Ltd, Worcestershire, U.K.) and were quantified by laser Doppler velocimetry as electrophoretic mobility using a disposable electrophoretic cell (DTS1061, Malvern Ltd., Worcestershire, U.K.). A total of 10 runs of 30 s were performed for each measurement, and four measurements were carried out for each sample. Zeta average values were obtained by suspending the dry powders in the same media at a concentration of 1.0 mg/mL. A total of 20 runs of 30 s each were performed for each measurement and for each sample.

https://dx.doi.org/10.1021/acsomega.9b04354
ACS Omega 2020, 5, 6598−6610

Transmission and Scanning Electron Microscopy Analyses. Sample morphology and size in a dry state were analyzed on an FEI Tecnai F20 transmission electron microscope equipped with a Schottky emitter and operating at 120 and 200 keV. A total of 10 μL of the material suspended in deionized water at 10.0 mg/mL was dissolved in 5 mL of isopropanol and treated with ultrasound. A droplet of the resulting finely dispersed suspensions was evaporated at room temperature and under the atmospheric pressure on a holey film supported on a copper grid. For SEM analysis (FEI Quanta 200, Eindhoven, The Netherlands), nanoparticles were placed on a carbon tape and then gold-coated using a Sputter Coater E5100 (Polaron Equipment, Watford, Hertfordshire, U.K.) at 30 mA under argon at 10^{-3} mbar for 4 min. For SEM−EDX analysis, samples were deposited on a flat, mirror-polished silicon wafer mounted on an aluminum SEM stub and analyzed through an EDX microanalysis detector (INCA Energy 300, Oxford Instruments, Abingdon-on-Thames, U.K.). The microanalysis was performed in four different regions of the samples on squared areas of 2 μm × 2 μm at an acceleration voltage of 10 keV and was carried out at 5000× magnification.

Thermogravimetric Analysis. TGA was performed using an STA 449F3 Jupiter (Netzsch GmbH, Selb, Germany) apparatus. About 10 mg of the sample was weighted in an alumina crucible and heated from room temperature to 1100 °C under an air flow with a heating rate of 10 °C/min.

Crop Growth, Productivity, and Abiotic Stress Resistance. The early growth and abiotic stress resistance of maize (i.e., *Z. mays*) were evaluated with a pot experiment (0.0123 m^2) using a regular growth chamber (16 h/8 h light/dark cycle at 23 °C). The same amount of NK fertilizers (N, 211.3 mg, urea; K, 129.2 mg, KCl) was used in all of the tested conditions, while twice the amount of FS (184.6 mg) was used with respect to HA−HS nanoparticles (92.3 mg). Early growth rates of maize were assessed in terms of height and fresh and dry weights. Dry weights were measured after 2 day incubation of the fresh biomass at 60 °C until a constant weight was reached. The biomass increase per unit of P in fertilizers was calculated based on the ICP quantification of HA and humic-coated HA. Some nutritional elements (i.e., K, Ca, Fe, and P) of maize at an early growth stage were assessed based on ICP-OES analysis of the dried crop powders that were mechanically ground and then completely digested with an acid solution containing distilled water, 60% $HClO_4$, and H_2SO_4 (1:9:5 v/v/v ratio) at 300 °C for approximately 6 h. Salt stress experiments were also conducted under the same conditions as above, but soils (970.0 g) were premixed with sodium chloride (3.0 g) and maize seedlings pregrown in a bed soil were transferred to the salty soils.

Long-term maize corn productivity and P nutrient use efficiency were measured on pot cultivation of *Z. mays* (0.05 m^2) in a greenhouse for approximately 3 months. NPK treatments (i.e., urea (860.0 mg), FS (751.7 mg), and KCl (525.8 mg)) were performed as recommended by the Rural Development Administration in South Korea. Experiments with HA and HA−HS were performed as already described for early growth experiments, i.e., replacing FS with half the quantity of nanoparticles. Dry weights of the fully grown maize were measured after 3 day incubation at 70 °C, and their P contents in detail were assessed through vanado-molybdate-based colorations of phosphate ions derived from the acid digestion of finely ground maize powders as already described above. The physicochemical characteristics of soils used for all of the maize cultivation experiments are shown in Table S1.

Soil Microbiome Analysis. Soils near maize roots were collected at the harvest for the early growth experiments and stored at −75 °C for further DNA extraction. Metagenomic DNA extraction was performed with a FastDNA Spin Kit for Soil (MP Biomedicals). Polymerase chain reaction primers to obtain bacterial 16S rDNA amplicon were 341F (5′-CCTACGGGNGGCWGCAG-3′) and 805R (5′-GACTACHVGGGTATCTAATCC-3′). The PCR products were then purified with an Agencourt AMPure XP reagent bead and sequenced with a MiSeq 250 paired-end system (Illumina). FLASH (Fast Length Adjustment of SHort reads, v1.2.11)-based sequence assembly was employed. Operational taxonomic units (OTUs) were obtained by CD-HIT-OTU (http://weizhongli-lab.org/cd-hit-otu/)-based clustering DNA sequences showing greater than 97% sequence homology. Representative OTUs were assigned to corresponding species (query coverage > 85% and identity > 85%) with the NCBI 16S microbial database using the BLASTN v. 2.4.0+ algorithm.

■ ASSOCIATED CONTENT

Supporting Information

The Supporting Information is available free of charge at https://pubs.acs.org/doi/10.1021/acsomega.9b04354.

Photographic image, fresh/dry weight, and height of *Z. mays* treated with the nanoparticles in normal or salty soils; soil properties, OUT counting of *Xanthomonadaceae* and *Rhizobiaceae*, and known relatedness of selected microbial species with plants (PDF)

■ AUTHOR INFORMATION

Corresponding Authors

Jong-Rok Jeon − *Department of Agricultural Chemistry and Food Science & Technology and IALS, Gyeongsang National University, Jinju 52828, Republic of Korea;* orcid.org/0000-0002-5815-7815; Phone: +82-55-772-1962; Email: jrjeon@gnu.ac.kr; Fax: +82-55-772-1969

Alessio Adamiano − *Institute of Science and Technology for Ceramics (ISTEC), National Research Council (CNR), 48018 Faenza, Italy;* orcid.org/0000-0002-2077-0411; Phone: +39-0546-699-724; Email: alessio.adamiano@istec.cnr.it; Fax: +39-0546-699-799

Authors

Ho Young Yoon − *Department of Agricultural Chemistry and Food Science & Technology, Gyeongsang National University, Jinju 52828, Republic of Korea*

Jeong Gu Lee − *Department of Agricultural Chemistry and Food Science & Technology and Division of Applied Life Science (BK21Plus), Gyeongsang National University, Jinju 52828, Republic of Korea*

Lorenzo Degli Esposti − *Institute of Science and Technology for Ceramics (ISTEC), National Research Council (CNR), 48018 Faenza, Italy*

Michele Iafisco − *Institute of Science and Technology for Ceramics (ISTEC), National Research Council (CNR), 48018 Faenza, Italy*

Pil Joo Kim − *Department of Agricultural Chemistry and Food Science & Technology, Division of Applied Life Science*

https://dx.doi.org/10.1021/acsomega.9b04354
ACS Omega 2020, 5, 6598−6610

(BK21Plus), and IALS, Gyeongsang National University, Jinju 52828, Republic of Korea

Seung Gu Shin − *Department of Energy Engineering, Future Convergence Technology Research Institute, Gyeongnam National University of Science and Technology, Jinju 52725, Republic of Korea*

Complete contact information is available at: https://pubs.acs.org/10.1021/acsomega.9b04354

Notes

The authors declare no competing financial interest.

■ ACKNOWLEDGMENTS

H.Y.Y. and J.-R.J. were supported by "R&D Program for Forest Science Technology (2017041B10-1919-BA01)" provided by the Korea Forest Service (Korea Forestry Promotion Institute), the Next-Generation BioGreen 21 Program (SSAC, Grant No. PJ01319501) of Rural Development Administration, and the National Research Foundation of Korea (NRF) grant funded by the Korea government (MSIT) (No. 2019R1C1C1008313). A.A. and M.I. thank the Italian Embassy of Seoul for providing travel funding to the Republic of Korea.

■ REFERENCES

(1) Guo, J. H.; Liu, X. J.; Zhang, Y.; Shen, J. L.; Han, W. X.; Zhang, W. F.; Christie, P.; Goulding, K. W. T.; Vitousek, P. M.; Zhang, F. S. Significant acidification in major Chinese croplands. *Science* **2010**, *327*, 1008−1010.

(2) Meijl, H.; Havlik, P.; Lotze-Campen, H.; Stehfest, E.; Witzke, P.; Dominguez, I. P.; Bodirsky, B. L.; Dijk, M. V.; Doelman, J.; Fellmann, T.; Humpenoder, F.; Koopman, J.; Muller, C.; Popp, A.; Tabeau, A.; Valin, H.; Zeist, W. Comparing impacts of climate change and mitigation on global agriculture by 2050. *Envrion. Res. Lett.* **2018**, *13*, No. 064021.

(3) Singh, A. Soil salinization and waterlogging: A threat to environment and agricultural sustainability. *Ecol. Indic.* **2015**, *57*, 128−130.

(4) United Nations (UN). *World Population Projected to Reach 9.7 Billion by 2050*; UN: New York, 2015; http://www.un.org/en/development/desa/news/population/2015-report.html (accessed March 1, 2017).

(5) Servin, A. D.; Morales, M. I.; Castillo-Michel, H.; Hernandez-Viezcas, J. A.; Munoz, B.; Zhao, L.; Nunez, J. E.; Peralta-Videa, J. R.; Cardea-Torresdey, J. L. Synchrotron verification of TiO_2 accumulation in cucumber fruit: A possible pathway of TiO_2 nanoparticle transfer from soil into the food chain. *Environ. Sci. Technol.* **2013**, *47*, 11592−11598.

(6) Samavini, R.; Sandaruwan, C.; Silva, M. D.; Priyadarshana, G.; Kottegoda, N.; Karunaratne, V. Effect of citric acid surface modification on solubility of hydroxyapatite nanoparticles. *J. Agric. Food Chem.* **2018**, *66*, 3330−3337.

(7) Liu, R.; Lal, R. Effects of molecular weight and concentration of carboxymethyl cellulose on morphology of hydroxyapatite nanoparticles as prepared with one-step wet chemical method. *Front. Environ. Sci. Eng.* **2015**, *9*, 804−812.

(8) Kottegoda, N.; Sandaruwan, C.; Priyadarshana, G.; Siriwardhana, A.; Rathnayake, U. A.; Berugoda Arachchige, D. M.; Kumarasinghe, A. R.; Dahanayake, D.; Karunaratne, V.; Amaratunga, G. A. Urea-hydroxyapatite nanohybrids for slow release of nitrogen. *ACS Nano* **2017**, *11*, 1214−1221.

(9) Chung, J. E.; Tan, S.; Gao, S. J.; Yongvongsoontorn, N.; Kim, S. H.; Lee, J. H.; Choi, H. S.; Yano, H.; Zhuo, L.; Kurisawa, M.; Ying, J. Y. Self-assembled micellar nanocomplexes comprising green tea catechin derivatives and protein drugs for cancer therapy. *Nat. Nanotechnol.* **2014**, *9*, 907−912.

(10) Gao, Y.; Wu, X.; Zhou, L.; Su, Y.; Dong, C. M. A sweet polydopamine nanoplatform for synergitic combination of targeted chemo-photothermal therapy. *Macromol. Rapid Commun.* **2015**, *36*, 916−922.

(11) Jeong, H. J.; Cha, J. Y.; Choi, J. H.; Jang, K. S.; Lim, J.; Kim, Y. W.; Seo, D. C.; Jeon, J. R. One-pot transformation of technical lignins into humic-like plant stimulants through Fenton-based advanced oxidation: Accelerating natural fungus-driven humification. *ACS Omega* **2018**, *3*, 7441−7453.

(12) Savy, D.; Mazzei, P.; Drosos, M.; Cozzolino, V.; Lama, L.; Piccolo, A. Molecular characterization of extracts from biorefinery wastes and evaluation of their plant biostimulation. *ACS Sustainable Chem. Eng.* **2017**, *5*, 9023−9031.

(13) Garcia, A. C.; de Souza, L. G.; Pereira, M. G.; Castro, R. N.; Garcia-Mina, J. M.; Zonta, E.; Lisboa, F. J.; Berbara, R. L. Structure-property-function relationship in humic substances to explain the biological activity in plants. *Sci. Rep.* **2016**, *6*, No. 20798.

(14) Vekariya, R. L.; Sonigara, K. K.; Fadabu, K. B.; Vaghasiya, J. V.; Soni, S. S. Humic acid as a sensitizer in highly stable dye solar cells: energy from an abundant natural polymer soil component. *ACS Omega* **2016**, *1*, 14−18.

(15) Raliya, R.; Saharan, V.; Dimkpa, C.; Biswas, P. Nanofertilizer for precision and sustainable agriculture: current state and future perspectives. *J. Agric. Food Chem.* **2018**, *66*, 6487−6503.

(16) Liu, R.; Lal, R. Synthetic apatite nanoparticles as a phosphorus fertilizer for soybean (*Glycine max*). *Sci. Rep.* **2015**, *4*, No. 5686.

(17) Marchiol, L.; Filippi, A.; Adamiano, A.; Degli Esposti, L.; Lafisco, M.; Mattiello, A.; Petrussa, E.; Braidot, E. Influence of hydroxyapatite nanoparticles on germination and plant metabolism of tomato (*Solanum lycopersicum* L.): Preliminary evidence. *Agronomy* **2019**, *9*, 161.

(18) Adamiano, A.; Sangiorgi, N.; Sprio, S.; Ruffini, A.; Sandri, M.; Sanson, A.; Gras, P.; Grossin, D.; Francès, C.; Chatzipanagis, K.; Bilton, M.; Marzec, B.; Varesano, A.; Meldrum, F.; Kröger, R.; Tampieri, A. Biomineralization of a titanium-modified hydroxyapatite semiconductor on conductive wool fibers. *J. Mater. Chem. B* **2017**, *5*, 7608−7621.

(19) Sakhno, Y.; Burtinetti, L.; Iafisco, M.; Tampieri, A.; Roveri, N.; Martra, G. Surface Hydration and Cationic Sites of Nanohydroxyapatites with Amorphous or Crystalline Surfaces: A Comparative Study. *J. Phys. Chem. C* **2010**, *114*, 16640−16648.

(20) Marrella, A.; Iafisco, M.; Adamiano, A.; Rossi, S.; Alello, M.; Barandalla-Sobrados, M.; Carullo, P.; Miragoli, M.; Tampieri, A.; Scaglione, S.; Catalucci, D. A. A combined low-frequency electromagnetic and fluidic stimulation for a controlled drug release from superparamagnetic calcium phosphate nanoparticles: potential application for cardiovascular diseases. *J. R. Soc., Interface* **2018**, *15*, No. 20180236.

(21) Edwards, G. A.; Amirtharajah, A. Removing color caused by humic acids. *J. - Am. Water Works Assoc.* **1985**, *77*, 50−57.

(22) Aeschbacher, M.; Graf, C.; Schwarzenbach, R. P.; Sander, M. Antioxidant properties of humic substances. *Environ. Sci. Technol.* **2012**, *46*, 4916−4925.

(23) Jekel, M. R. The stabilization of dispersed mineral particles by adsorption of humic substances. *Water Res.* **1986**, *20*, 1543−1554.

(24) Andreani, T.; Miziara, L.; Lorenzon, E.; Souza, A. L.; Kiill, C. P.; Fangueiro, J. F.; Garcia, M. L.; Gremiao, P. D.; Silva, A. M.; Souto, E. B. Effect of mucoadhesive polymers on the in vitro performance of insulin-loaded silica nanoparticles: Interactions with mucin and biomembrane models. *Eur. J. Pharm. Biopharm.* **2015**, *93*, 118−126.

(25) Tatzber, M.; Stemmer, M.; Spiegel, H.; Katzlberger, C.; Haberhauer, G.; Mentler, A.; Gerzabek, M. H. FTIR-spectroscopic characterization of humic acids and humic fractions obtained by advanced NaOH, $Na_4P_2O_7$, and Na_2CO_3 extraction procedures. *J. Plant Nutr. Soil Sci.* **2007**, *170*, 522−529.

(26) Wang, Y.; Michel, F. M.; Choi, Y. S.; Eng, P. J.; Levard, C.; Siebner, H.; Gu, B.; Barger, J. R.; Brown, G. E., Jr. Pb, Cu, and Zn distributions at humic acid-coated metal-oxide surfaces. *Geochim. Cosmochim. Acta* **2016**, *188*, 407−423.

(27) Kurita, K.; Sannan, T.; Iwakura, Y. Studies on chitin. VI. Binding of metal cations. *J. Appl. Polym. Sci.* **1979**, *23*, 511−515.
(28) Lee, J. G.; Yoon, H. Y.; Cha, J.-Y.; Kim, W.-Y.; Kim, P. J.; Jeon, J.-R. Artificial humification of lignin architecture: Top-down and bottom-up approaches. *Biotechnol. Adv.* **2019**, *37*, 107416.
(29) Jeon, J. R.; Kim, E. J.; Murugesan, K.; Park, H. K.; Kim, Y. M.; Kwon, J. H.; Kim, W. G.; Lee, J. Y.; Chang, Y. S. Laccase-catalyzed polymeric dye synthesis from plant-derived phenols for potential application in hair dyeing: Enzymatic colorations driven by homo- or hetero-polymer synthesis. *Microb. Biotechnol.* **2010**, *3*, 324−335.
(30) Mollazadeh, S.; Javadpour, J.; Khavandi, A. In situ synthesis and characterization of nano-size hydroxyapatite in poly(vinyl alcohol) matrix. *Ceram. Int.* **2007**, *33*, 1579−1583.
(31) Delgado, A.; Madrid, A.; Kassem, S.; Andrew, L.; del Campillo, M. C. Phosphorus fertilizer recovery from calcareous soils amended with humic and fulvic acids. *Plant Soil* **2002**, *245*, 277−286.
(32) Bezuglova, O. S.; Gorovtsov, A. V.; Polienko, E. A.; Zinchenko, V. E.; Grinko, A. V.; Lykhman, V. A.; Dubinina, M. N.; Demidov, A. Effect of humic preparation on winter wheat productivity and rhizosphere microbial community under herbicide-induced stress. *J. Soils Sediments* **2019**, 2665−2675.
(33) Deng, S.; Bai, R. Adsorption and desorption of humic acid on aminated polyacrylonitrile fibers. *J. Colloid Interface Sci.* **2004**, *280*, 36−43.
(34) Muscolo, A.; Sidari, M.; Nardi, S. Humic substance: Relationship between structure and activity. Deeper information suggests univocal findings. *J. Geochem. Explor.* **2013**, *129*, 57−63.
(35) Sindelar, H. R.; Brown, M. T.; Boyer, T. H. Effect of natural organic matter on calcium and phosphorus co-precipitation. *Chemosphere* **2015**, *138*, 218−224.
(36) Deryng, D.; Conway, D.; Ramankutty, N.; Price, J.; Warren, R. Global crop yield response to extreme heat stress under multiple climate change futures. *Envrion. Res. Lett.* **2014**, *9*, No. 034011.
(37) Khaleda, L.; Park, H. J.; Yun, D. J.; Jeon, J. R.; Kim, M. G.; Cha, J. Y.; Kim, W. Y. Humic acid confers high-affinity K+ transporter 1-mediated salinity stress tolerance in Arabidopsis. *Mol Cells* **2017**, *40*, 966.
(38) Pinton, R.; Cesco, S.; De Nobili, M.; Santi, S.; Varanini, Z. Water- and pyrophosphate-extractable humic substances fractions as a source of iron for Fe-deficient cucumber plants. *Biol. Fertil. Soils* **1997**, *26*, 23−27.
(39) Verlinden, G.; Pycke, B.; Mertens, J.; Debersaques, F.; Verheyen, K.; Baert, G.; Bries, J.; Haesaert, G. Application of humic substances results in consistent increases in crop yield and nutrient uptake. *J. Plant Nutr.* **2009**, *32*, 1407−1426.
(40) Zhang, R.; Vivanco, J. M.; Shen, Q. The unseen rhizosphere root-soil-microbe interactions for crop production. *Curr. Opin. Microbiol.* **2017**, *37*, 8−14.
(41) Lovley, D. R.; Coates, J. D.; Blunt-Harris, E. L.; Philips, E. J. P.; Woodward, J. C. Humic substances as electron acceptors for microbial respiration. *Nature* **1996**, *382*, 445−448.
(42) Dilly, O. Effects of glucose, cellulose, and humic acids on soil microbial eco-physiology. *J. Plant Nutr. Soil Sci.* **2004**, *167*, 261−266.
(43) Singh, H.; Khattar, J. S.; Ahluwalia, A. S. Cyanobacteria and agricultural crops. *Vegetos* **2014**, *27*, 37−44.
(44) Li, X.; Rui, j.; Mao, Y.; Yannarell, A.; Mackie, R. Dynamics of the bacterial community structure in the rhizosphere of a maize cultivar. *Soil Biol. Biochem.* **2014**, *68*, 392−401.
(45) Peix, A.; Rivas-Boyero, A. A.; Mateos, P. F.; Rodriguez-Barrueco, C.; Martinez-Molina, E.; Velazquez, E. Growth promotion of chickpea and barley by a phosphate solubilizing strain of Mesorhizobium mediterraneum under growth chamber conditions. *Soil Biol. Biochem.* **2001**, *33*, 103−110.
(46) Colomb, B.; Kinirym, J. R.; Debaeke, P. Effect of soil phosphorus on leaf development and senescence dynamics of field-grown maize. *Agron. J.* **2000**, *92*, 428−435.
(47) Singh, V.; Pallaghy, C. K.; Singh, D. Phosphorus nutrition and tolerance of cotton to water stress. I. Seed cotton yield and leaf morphology. *Field Crops Res.* **2006**, *96*, 191−198.

https://dx.doi.org/10.1021/acsomega.9b04354
ACS Omega 2020, 5, 6598−6610